Photonic ultra-wideband monocycle pulses generation using semiconductor optical amplifier and electro-absorber in parallel

Bingbing Wu (吴冰冰)*, Jian Wu (伍 剑), Kun Xu (徐 坤), Xiaobin Hong (洪小斌), Junyi Zhang (张君毅), and Jintong Lin (林金桐)

Key Laboratory of Information Photonics & Optical Communications, Beijing University of Posts and Telecommunications, Beijing 100876, China

**E-mail: wubingbing416@163.com*

Received May 31, 2010

A scheme for photonic generation of ultra-wideband (UWB) pulses using a semiconductor optical amplifier (SOA) and an electro-absorber (EA) in parallel is proposed and numerically demonstrated. By adjusting the time delay between two pump signals incident into the SOA and the EA, we can obtain monocycle pulses with reversed polarities and different bandwidths. The proposed method is flexible in pulse shaping and easy in practical optimization.

OCIS codes: 350.4010, 250.5980, 070.4340.

doi: 10.3788/COL20100809.0902.

Ultra-wideband (UWB) impulse radio is considered to be a promising solution to sensors and high-speed short-distance wireless access networks[1]. It takes advantages of low power consumption, immunity to multi-path fading, high security, and feasibility of sharing bandwidth with existing radio systems. Recently, photonic generation of UWB signal attracts intensive discussions; in particular, semiconductor optical amplifier (SOA) based schemes[2−7] and electro-absorber (EA) based schemes[7,8] have attracted considerable interest due to their compactness, low-power consumption, and ease integration. Most of the previous schemes are limited to single-polarity[2,4,8] or fixed-bandwidth[2,3,6,8] monocycle UWB pulse generation. Based on cross-polarization modulation (XPolM), monocycle pulses with reversed polarities can be obtained[5]. However, it is sensitive to polarization. In Ref. [7], a cascade scheme of SOA and EA is used to generate UWB monocycle pulse, an additional optical band-pass filter (OBPF) with 1-nm bandwidth is inserted between the SOA and the EA to block the forward and the backward propagating pump signals. Since the power level of the pump signal after passing though the SOA is high, it may affect nonlinear interaction in the subsequent EA if the OBPF is not perfect enough. Also, the wavelength range of the probe signal is limited by the used OBPF. In this letter, an approach to photonic generation of UWB pulses using a SOA and an EA in parallel is proposed and numerically demonstrated. By adjusting the time delay between two pump signals incident into the SOA and the EA, we can achieve monocycle pulses with reversed polarities. The monocycle pulse shape and bandwidth can be flexibly adjusted and easily optimized.

The principle of the proposed UWB generation approach is illustrated in Fig. 1. A continuous-wave (CW) light at the wavelength of λ_1 is modulated by a Mach-Zehnder modulator (MZM) to produce positive Gaussian pulse train in a fixed pattern. After amplification, the signal is split into two beams to serve as pump signals in SOA and EA links, respectively. Two additional CW lights at λ_2 and λ_3 act as probe signals of SOA and EA links.

As shown in Fig. 1(b), in the SOA link, thanks to cross-gain modulation (XGM) effect the CW probe signal at λ_2 is modulated to negative Gaussian shape by the pump signal. While opposite modulation property is behaved by EA, and the CW probe signal at λ_3 is modulated to positive Gaussian shape by cross-absorption modulation (XAM) effect. Then the two polarity-reversed Gaussian pulses are filtered out and combined to compose the monocycle UWB pulse. The polarity and the shape of the generated UWB pulse can be flexibly adjusted by regulating the delay time between two pump signals.

Now we present the theoretical models for analyzing

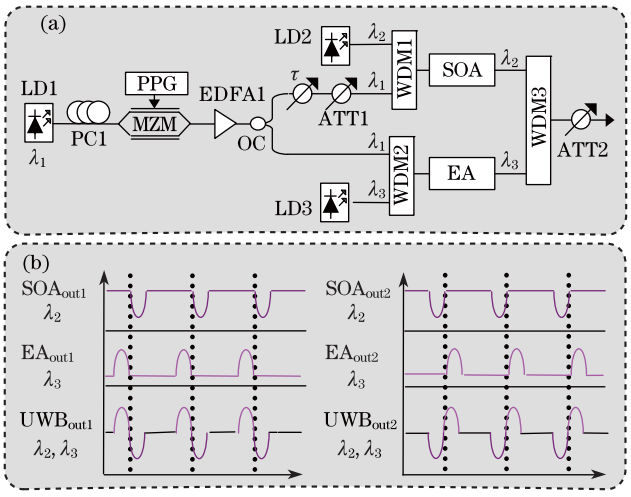

Fig. 1. (a) Setup for the proposed UWB pulse generation scheme (LD: laser diode, PC: polarization controller; PPG: pulse pattern generator; WDM: wavelength-division multiplexing; EDFA: erbium-doped fiber amplifier; OC: optical coupler; ATT: attenuator); (b) schematic illustration of the operational principle.

optical wave propagation in SOA and EA, respectively. Figure 2 presents the configuration considered in our model. A pump signal at the wavelength of λ_1 and a CW probe signal at the wavelength of λ_2 (λ_3) are injected into the SOA (EA). Dividing the SOA and the EA into a number of uniform sections, then the considered information in each subsection i could be evaluated. The backbone of our theoretical model includes two parts: the wave propagation for all waves and the amplified spontaneous emission (ASE), and the material dynamic process. The former part is solved by the coupled-mode equations, while the latter part is described by the carrier rate equation.

The SOA is divided into $M_{\rm SOA}$ subsections along the longitudinal direction. The propagation and nonlinear interaction between two signals in each subsection i could be expressed by the coupled-mode equation[9,10]:

$$\frac{{\rm d}A_{k,i}}{{\rm d}z} = \frac{1}{2}\left[\frac{\Gamma g_{k,i}}{1+P_i/P_{\rm s}}(1-i\alpha_p)-\alpha_l\right]A_{k,i}, \quad (1)$$

where $A_{k,i}$ denotes the slowly varying envelope of the optical field inside subsection i, subscripts k=1, 2 stand for the two input signals; Γ is the mode confinement factor; α_p is the linewidth enhancement factor; α_l is the internal loss; $P_{\rm s}$ is saturation power of the SOA; and $P_i = \sum |A_{k,i}|^2$ is the total optical power inside i subsection. $g_{k,i}$ represents the material gain coefficient of the SOA which is both carrier and wavelength dependent, and can be approximated by[9]

$$\begin{aligned} g_{k,i} = {} & b_1(N_i - N_{\rm ref}) - b_2[\lambda_k - \lambda_{\rm ref} + b_4(N_i - N_{\rm ref})]^2 \\ & + b_3[\lambda_k - \lambda_{\rm ref} + b_4(N_i - N_{\rm ref})]^3, \end{aligned} \quad (2)$$

where b_1, b_2, and b_3 are gain constants; b_4 is the gain peak shift coefficient; $N_{\rm ref}$ represents the referential carrier density; $\lambda_{\rm ref}$ denotes the referential peak-gain wavelength; λ_k is the wavelength of the optical wave in consideration. N_i stands for the carrier density in subsection i, and it can be expressed by the following carrier rate equation[9]:

$$\begin{aligned} \frac{{\rm d}N_i}{{\rm d}t} = {} & \frac{I}{edLW} - (c_1 N_i + c_2 N_i^2 + c_3 N_i^3) \\ & - \frac{\Gamma}{hcdW}\Big(\sum_k \lambda_k g_{k,i} |A_{k,i}|^2\Big) \\ & - \frac{2\Gamma}{hcdW}\Big[\sum_{k'=0}^{N_m-1} \lambda_{k'} g_{k',i} K_{k'} (P^+_{{\rm ASE}k',i} + P^-_{{\rm ASE}k',i})\Big], \end{aligned} \quad (3)$$

where I refers to the bias current; e is the electron charge; c_1, c_2, and c_3 are recombination coefficients; dLW represents the volume of the active region in the SOA; $P^+_{{\rm ASE}k',i}$ and $P^-_{{\rm ASE}k',i}$ represent the forward and the backward propagating ASEs[9]. Equation (3) reveals that the variation of carrier density is induced by additional carriers to the active region from the bias current, radiative and nonradiative carrier recombination rates, carrier consumption induced by the stimulated emission of all considered waves and the ASE.

The EA is divided into $M_{\rm EA}$ subsections along the longitudinal direction. The propagation and nonlinear interaction between the pump and the probe signals in each subsection j could be described by the coupled-mode equation[11,12]:

$$\frac{{\rm d}A_{m,j}}{{\rm d}z} = -\frac{1}{2}[\Gamma\alpha_j + \alpha_l]A_{m,j}, \quad (4)$$

where $A_{m,j}$ is the slowly varying envelope of the optical field inside subsection j, subscripts m=1, 2 stand for two optical signals; α_l is the internal loss. The absorption coefficient α_j could be expressed as[11,12]

$$\alpha_j = \frac{\alpha_0}{1+\varepsilon_{{\rm supp}P_j}}[1 - f_{\rm e}(\varepsilon^0_{\rm e}) - f_{\rm h}(\varepsilon^0_{\rm h})], \quad (5)$$

where α_0 represents the unsaturated absorption coefficient; $\varepsilon_{\rm supp}$ is the absorption suppression factor; $P_j = \sum |A_{m,j}|^2$ is the total optical power inside j subsection; $f_{\rm e}$ and $f_{\rm h}$ are the Fermi distributions characterized by the temperatures and Fermi levels[11]. The temperatures here are assumed to be constant, and equal to the lattice temperature.

The dynamics of Fermi levels are related to the carrier density $N_{p,j}$ (p = e, h refer to the electron in conduction band and hole in valence band, rerpectively), which could be described as

$$\frac{{\rm d}N_{p,j}}{{\rm d}t} = \frac{\Gamma\alpha_j}{hcdW}\Big(\sum_m \lambda_m |A_{m,j}|^2\Big) - \frac{N_{p,j}}{\tau_p}, \quad (6)$$

where $\tau_p (p = {\rm e}, {\rm h})$ denotes the carrier sweep-out time. The first term on the right-hand side of Eq. (6) describes the pumping rate of carriers into the absorbing region, and the second term represents interband carriers relaxation.

Therefore, the coupled-mode equation and carrier density rate equation are a comprehensive set of finalized equations both in our SOA and EA models. After calculating the above equations, the slowly varying envelopes for all waves and the carrier density distributions in the SOA and the EA can be derived, respectively. Typical values of the parameters used in our SOA[9,10] and EA[11,12] models are summarized in Tables 1 and 2.

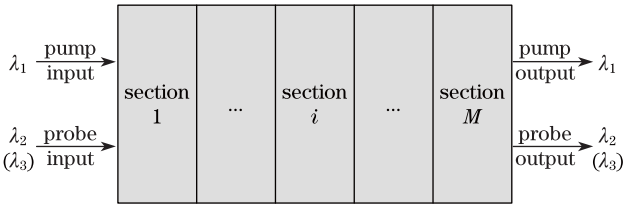

Fig. 2. Schematic diagram for optical signals transmission in a SOA or an EA.

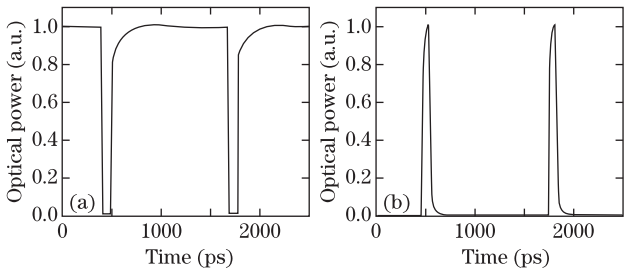

Fig. 3. Output probe signals after (a) SOA and (b) EA.

The lights from three LDs are emitted at λ_1= 1556.0 nm, λ_2=1559.2 nm, and λ_3=1560.0 nm, respectively. The CW light with the wavelength of λ_1 is modulated by a MZM to generate pump signals. The initial electrical Gaussian pulse signal to drive MZM is in a fixed pattern (one "1" per 16 bits) and at a bit rate of 12.5 Gb/s, indicating that the repetition rate of the generated pump Gaussian pulse train is 781.25 MHz. Then based on the SOA and the EA models described above, the proposed UWB generation scheme is numerically demonstrated. The modulated negative and positive Gaussian pulses after the SOA and the EA are presented in Fig. 3. Due to the slow carrier recovery of the SOA, the modulated negative Gaussian pulse holds a long trail in the leading edge. While the trail of EA output in the falling edge originates from the carrier sweep-out time.

Table 1. Parameters of the SOA

Symbol	Description	Value
L	Length of SOA Active Region	1.0×10^{-3} m
W	Width of SOA Active Region	3.3×10^{-6} m
d	Thickness of SOA Active Region	0.15×10^{-6} m
I	Bias Current	160 mA
$n_{\rm eq}$	Equivalent Refractive Index	3.22
$K_{k'}$	Filter Factor	1
c_1	Non-Radiative Recombination Constant	2.5×10^{8} s^{-1}
c_2	Bimolecular Recombination Constant	1×10^{-16} m^3·s^{-1}
c_3	Auger Recombination Constant	9.4×10^{-41} m^6·s^{-1}
b_1	Gain Constant	2.5×10^{-20} m^2
b_2	Gain Constant	7.4×10^{18} m^{-3}
b_3	Gain Constant	3.155×10^{25} m^{-4}
b_4	Gain Peak Shift Coefficient	3.0×10^{-32} m^4
Γ	Mode Confinement Factor	0.3
α_p	Linewidth Enhancement Factor	6
α_l	Internal Loss of SOA	4.0×10^{3} m^{-1}
$P_{\rm sat}$	Saturation Power	1.0×10^{-3} W
$\lambda_{\rm ref}$	Referential Peak-Gain Wavelength	1605 nm
$N_{\rm ref}$	Referential Carrier Density	0.9×10^{24} m^{-3}

Table 2. Parameters of the EA

Symbol	Description	Value
L	Length of EA Active Region	150×10^{-6} m
W	Width of EA Active Region	3.5×10^{-6} m
d	Thickness of EA Active Region	0.1×10^{-6} m
$n_{\rm eq}$	Equivalent Refractive Index	3
Γ	Mode Confinement Factor	0.285
α_l	Internal Loss of EA	4.0×10^{2} m^{-1}
α_0	Unsaturated Absorption Coefficient	1.3×10^{5} m^{-1}
$\varepsilon_{\rm supp}$	Absorption Suppression Factor	2.0×10^{-24} m^{-3}
$\tau_{\rm e}$	Electron Sweep-Out Time	25×10^{-12} s
$\tau_{\rm h}$	Hole Sweep-Out Time	100×10^{-12} s
$N_{\rm ref}$	Referential Carrier Density	0.9×10^{24} m^{-3}
$T_{\rm L}$	Lattice Temperature	300 K
E_g	Bandgap Energy	1.48 eV
m_0	Electron Mass in Vacuum	9.1×10^{-31} kg
$m_{\rm e}$	Electron Mass in the Conduction Band	$0.067m_0$
$m_{\rm h}$	Hole Mass in the Valence Band	$0.34m_0$

The simulation results are summarized in Fig. 4. The radio frequency (RF) spectrum after attenuator ATT2 is discrete, and the envelope of which corresponds to the spectrum of the generated UWB pulse. When adjusting the time delay between two pump signals, we can achieve monocycle UWB pulses with different shapes and reversed polarities, as shown in Figs. 4(a) and (b). Correspondingly, the center frequency, 10-dB bandwidth and the fraction bandwidth are presented in Figs. 4(c) and (d). Different bandwidth in Fig. 4(c) is caused by the different time delay between the negative and positive Gaussian pulses. A small time delay leads to a large pulse superposition in the time domain. Therefore, narrower pulse duration in time domain corresponds to wider bandwidth in RF spectrum. The center frequency is calculated from the RF spectrum, it is the central point within the frequency range corresponding to 10-dB bandwidth. Therefore, center frequency, 10-dB bandwidth, and fraction bandwidth are all dependent on the variation of time delay.

To investigate the robustness of our scheme, the impact of the duty-cycle of the pump signals on the generated UWB pulse are studied. When the duty-cycle is set at 100%, 67%, 50%, and 33%, the output UWB pulses and the corresponding RF spectra are shown in Fig. 5. When the duty-cycle of the pump signal is 33%, the RF spectrum is 12.11 GHz, which is too broad to comply with the Federal Communications Commision of USA (FCC) definition. When the duty-cycle of the pump signal is 100%, 67%, and 50%, the 10-dB bandwidth is 6.8, 8.13, and 9.38 GHz, respectively, all within the FCC regulation. Therefore, it is feasible to generate a RF spectrum conforming to the FCC regulations when the duty-cycle

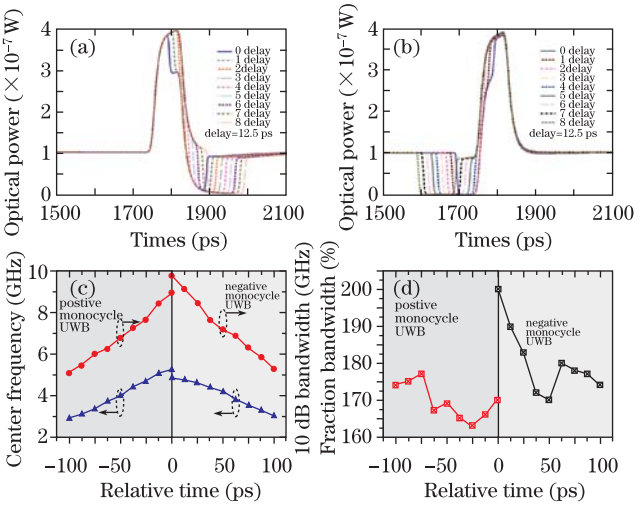

Fig. 4. Numerical results. (a) Positive monocycle pulse, (b) negative monocycle pulse, (c) center frequency and 10-dB bandwidth varying with different UWB pulse shapes, (d) fractional bandwidth varying with different UWB pulse shapes.

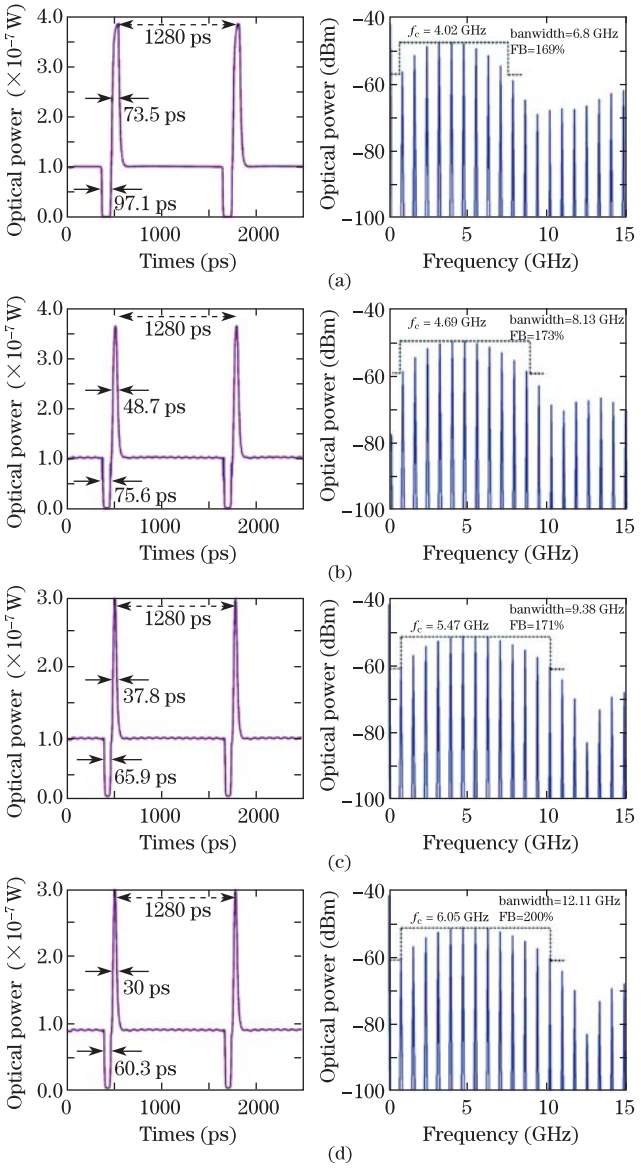

Fig. 5. Monocycle UWB pulses (left) and their RF spectra (right) when the duty-cycle of the pump signal is (a) 100%, (b) 67%, (c) 50%, and (d) 33%. FB: fraction bandwidth.

of the pump signal ranges from 50% to 100%.

In conclusion, an approach to photonic generation of UWB pulses using a SOA and an EA in parallel is proposed. Based on the theoretical SOA and EA models, the monocycle pulses with reversed polarities and different bandwidths are numerically demonstrated. The impact of the duty-cycle of the pump signals on the generated UWB pulse is also studied.

This work was partly supported by the National "863" program of China (Nos. 2009AA01Z256, 2009AA01Z253, and 2008AA01A331), the National Natural Science Foundation of China (Nos. 60736036, 60702006, 60837004, 60736002, and 60932004), the MOST program (No. 2008DFA11670), the Project Funded by the State Key Lab of AOCSN, China, the Excellent Doctoral Innovation Project funded by Beijing University of Posts and Telecommunications (No. CX201012), the Specialized Research Fund for the Doctoral Program of Higher Education (No. 200800131007), and the Fundamental Research Funds for the Central Universities.

References

1. G. R. Aiello and G. D. Rogerson, IEEE Microw. Mag. **4,** (2) 36 (2003).
2. Q. Wang, F. Zeng, S. Blais, and J. Yao, Opt. Lett. **31,** 3083 (2006).
3. J. Dong, X. Zhang, J. Xu, and D. Huang, Opt. Lett. **32,** 1223 (2007).
4. J. Dong, X. Zhang, J. Xu, and D. Huang, Opt. Lett. **32,** 2158 (2007).
5. H. Chen, M. Chen, T. Wang, M. Li, and S. Xie, J. Lightwave Technol. **26,** 2492 (2008).
6. W. Zhang, J. Sun, J. Wang, C. Cheng, and X. Zhang, IEEE Photon. Technol. Lett. **21,** 271 (2009).
7. E. Zhou, X. Zhang, X. Yu, J. Dong, W. Xue, and I. T. Monroy, in *Proceedings of OFC 2009* JWA49 (2009).
8. T. H. Wu, J. P. Wu, Y. F. Choi, and Y. J. Chiu, in *Proceedings of LEOS 2009* WO3 (2009).
9. H. Wang, J. Wu, and J. Lin, J. Lightwave Technol. **23,** 2761 (2005).
10. P. Li, D. Huang, X. Zhang, and G. Zhu, Opt. Express **14,** 11839 (2006).
11. A. V. Uskov, J. R. Karin, J. E. Bowers, J. G. McInerney, and J. L. Bihan, IEEE J. Quantum Electron. **34,** 2162 (1998).
12. E. J. M. Verdurmen, Y. Liu, G. D. Khoe, and H. de Waardt, IEE Proc.-Optoelectron. **153,** 75 (2006).